

Charge orders with distinct magnetic response in a prototypical kagome superconductor LaRu_3Si_2

C. Mielke III,^{1,2,*} V. Sazgari,^{1,*} I. Plokhikh,³ S. Shin,⁴ H. Nakamura,⁵ J.N. Graham,¹ J. Küspert,² I. Biało,² G. Garbarino,⁶ D. Das,¹ M. Medarde,⁴ M. Bartkowiak,⁷ S.S. Islam,¹ R. Khasanov,¹ H. Luetkens,¹ M.Z. Hasan,⁸ E. Pomjakushina,³ J.-X. Yin,⁹ M. H. Fischer,² J. Chang,² T. Neupert,² S. Nakatsuji,¹⁰ B. Wehinger,⁶ D.J. Gawryluk,^{3,†} and Z. Guguchia^{1,‡}

¹Laboratory for Muon Spin Spectroscopy, Paul Scherrer Institute, CH-5232 Villigen PSI, Switzerland

²Physik-Institut, Universität Zürich, Winterthurerstrasse 190, CH-8057 Zürich, Switzerland

³Laboratory for Multiscale Materials Experiments,
Paul Scherrer Institut, 5232, Villigen PSI, Switzerland

⁴Laboratory for Multiscale Materials Experiments,
Paul Scherrer Institut, CH-5232 Villigen PSI, Switzerland

⁵Institute for Solid State Physics (ISSP), University of Tokyo, Kashiwa, Chiba 277-8581, Japan

⁶European Synchrotron Radiation Facility, 71 Avenue des Martyrs, 38000 Grenoble, France

⁷Laboratory for Neutron and Muon Instrumentation,
Paul Scherrer Institut, CH-5232 Villigen, Switzerland

⁸Laboratory for Topological Quantum Matter and Advanced Spectroscopy (B7),
Department of Physics, Princeton University, Princeton, New Jersey 08544, USA

⁹Department of Physics, Southern University of Science and Technology, Shenzhen, Guangdong, 518055, China

¹⁰Institute for Solid State Physics, University of Tokyo, Kashiwa, 277-8581, Japan

The kagome lattice[1–4] has emerged as a promising platform for hosting unconventional chiral charge order at high temperatures. Notably, in LaRu_3Si_2 , a room-temperature charge-ordered state with a propagation vector of $(\frac{1}{4}, 0, 0)$ has been recently identified [5]. However, understanding the interplay between this charge order and superconductivity, particularly with respect to time-reversal-symmetry breaking, remains elusive. In this study, we employ single crystal X-ray diffraction, magnetotransport, and muon-spin rotation experiments to investigate the charge order and its electronic and magnetic responses in LaRu_3Si_2 across a wide temperature range down to the superconducting state. Our findings reveal the emergence of a charge order with a propagation vector of $(\frac{1}{6}, 0, 0)$ below $T_{\text{CO},2} \simeq 80$ K, coexisting with the previously identified room-temperature primary charge order $(\frac{1}{4}, 0, 0)$. The primary charge-ordered state exhibits zero magnetoresistance. In contrast, the appearance of the secondary charge order at $T_{\text{CO},2}$ is accompanied by a notable magnetoresistance response and a pronounced temperature-dependent Hall effect, which experiences a sign reversal, switching from positive to negative below $T^* \simeq 35$ K. Intriguingly, we observe an enhancement in the internal field width sensed by the muon ensemble below $T^* \simeq 35$ K. Moreover, the muon spin relaxation rate exhibits a substantial increase upon the ap-

plication of an external magnetic field below $T_{\text{CO},2} \simeq 80$ K. Our results highlight the coexistence of two distinct types of charge order in LaRu_3Si_2 within the correlated kagome lattice, namely a non-magnetic charge order $(\frac{1}{4}, 0, 0)$ below $T_{\text{CO},1} \simeq 400$ K and a time-reversal-symmetry-breaking charge order below $T_{\text{CO},2}$, coexisting with superconductivity. This study sheds light on the intricate electronic and magnetic phenomena occurring in kagome superconductors, providing valuable insights into their unique properties and potential applications.

Kagome superconductors [6–11], distinguished by their unique lattice structure resembling the traditional Japanese kagome pattern, exhibit diverse electronic behaviors and have become a focal point in the study of condensed matter physics. One intriguing aspect is their propensity to host chiral charge order [12–18], a phenomenon where the electron density is spatially modulated to give the system a handedness, introducing unconventional electronic states. Understanding this interrelationship between kagome superconductivity and chiral charge order is pivotal for harnessing their unique properties in the development of novel quantum materials and technologies.

Four distinct classes of kagome lattice systems have recently been identified as exhibiting charge order: the AV_3Sb_5 family (where $A = \text{K}, \text{Rb}, \text{Cs}$) [9–11], ScV_6Sn_6 [19, 20], FeGe [21, 22] and LaRu_3Si_2 [5]. In AV_3Sb_5 , a correlated interplay of charge order emerges below T_{co} (around 80-110 K), alongside a superconducting phase developing below T_c (approximately 1-3 K). ScV_6Sn_6 , sharing a similar vanadium structural motif with AV_3Sb_5 , displays charge order below T_{co} (around 90 K) but does not exhibit superconductivity down to

*These authors contributed equally to the paper.

†Electronic address: dariusz.gawryluk@psi.ch

‡Electronic address: zurab.guguchia@psi.ch

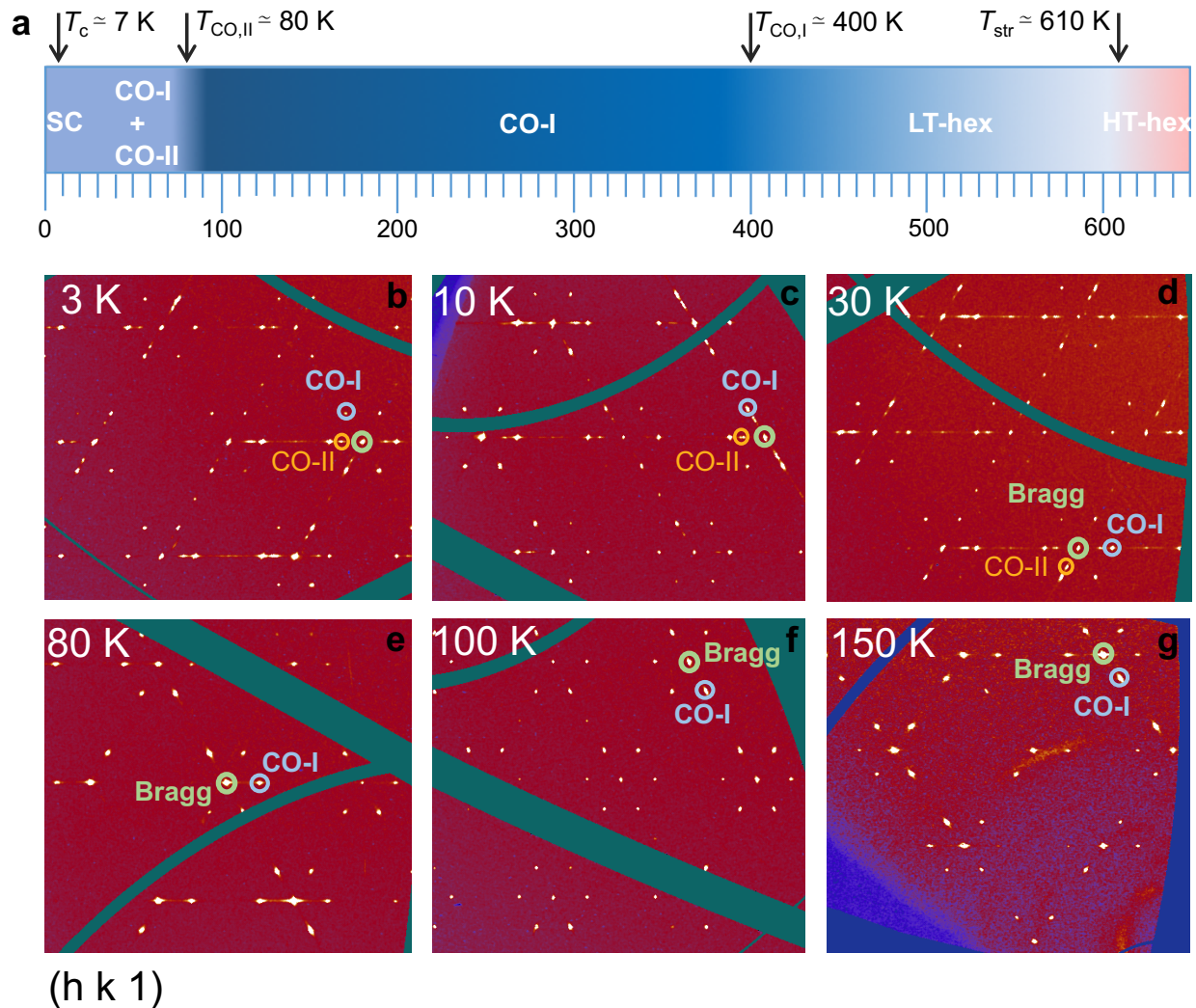


Figure 1: **Charge order in LaRu_3Si_2 .** **a**, Schematic phase diagram as a function of temperature of LaRu_3Si_2 . The arrows mark the structural phase transition temperature T_{str} from the high-temperature hexagonal $P6/mmm$ phase (SG No. 191) to the low-temperature orthorhombic $Cccm$ phase (SG No. 66), primary charge order transition temperature $T_{\text{CO-I}}$ and secondary charge order transition temperature $T_{\text{CO-II}}$. **b – g**, Reconstructed reciprocal space along the $(h k 1)$ direction, performed at various temperatures above and below the superconducting transition temperature.

the lowest measured temperatures. In contrast, FeGe , characterized as a correlated magnetic kagome system, demonstrates A-type antiferromagnetic order below 400 K and charge order below 100 K. One of the most remarkable features of the charge ordered state in all three materials is the emergence of possible time-reversal symmetry (TRS)-breaking, featuring both magnetic and electronic anomalies [12–17, 23–38]. Theoretical considerations suggest that these features may be explained by a complex order parameter, realizing a higher angular-momentum state, akin to unconventional superconducting orders. LaRu_3Si_2 stands out within the realm of

bulk kagome-lattice superconductors due to its exceptional characteristics. Notably, it boasts the highest superconducting critical temperature, reaching approximately 7 K [8, 39–42]. Furthermore, using single crystal X-ray diffraction we recently showed that LaRu_3Si_2 exhibits a charge-ordered state at temperatures above room temperature [5]. The coexistence of both high-temperature charge order and notable superconductivity makes LaRu_3Si_2 a particularly intriguing system for the exploration of quantum phenomena and potential applications in the field of condensed matter physics.

X-ray diffraction measurements on LaRu_3Si_2 have pre-

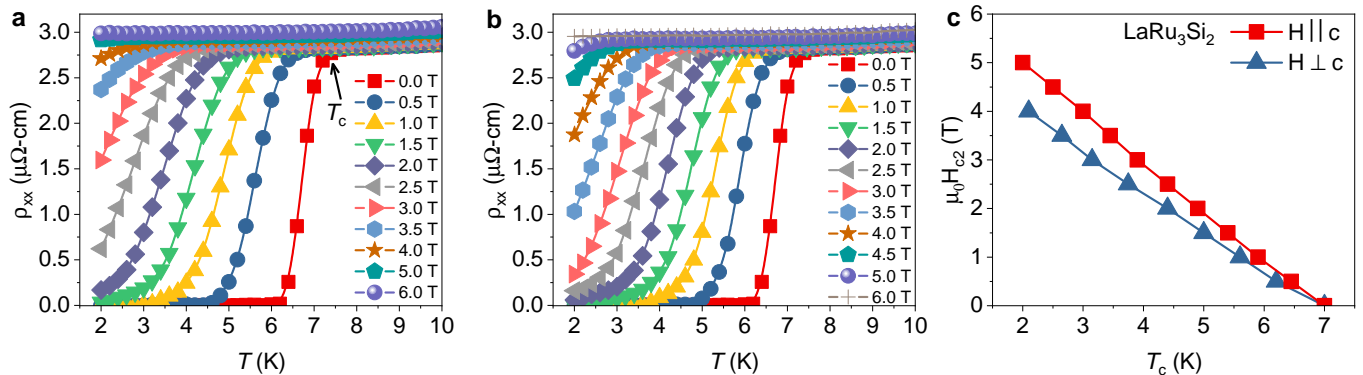


Figure 2: **Weakly anisotropic superconducting properties of LaRu₃Si₂.** The temperature dependence of the electrical resistivity of a single crystal of LaRu₃Si₂, measured under various magnetic fields applied perpendicular to the c -axis (a) and parallel to the c -axis (b). c, the magnetic field-temperature phase diagram is derived from the data shown in panels a and b.

viously [5] been constrained to temperatures above 80 K, leaving uncertainties regarding the persistence of charge order into the superconducting state. Additionally, a comprehensive understanding of the electronic and magnetic response in the normal state remained elusive. Here, we address these questions to gain insights into the charge order across a broad temperature range, encompassing the superconducting state, as well as to elucidate the electronic and magnetic behaviors in the normal state. We employ a set of techniques, including single crystal X-ray diffraction, magnetotransport measurements, and a combination of zero-field and high-field muon spin relaxation/rotation (μ SR) experiments on a single crystal of LaRu₃Si₂. This multifaceted experimental approach aims to provide a comprehensive understanding of the charge-order phenomena and associated electronic and magnetic responses in both the normal and superconducting states of LaRu₃Si₂. Studying the magnetic response of charge orders is crucial for understanding the underlying quantum phenomena and the role they play in the emergent properties of these materials.

In Figures 1b – g, we present reconstructed reciprocal-space patterns along the $(hk1)$ direction for various temperatures both above and below the superconducting critical temperature T_c , which is approximately 7 K, for a single crystal of LaRu₃Si₂. At a higher temperature, $T = 150$ K, the diffraction pattern reveals fundamental Bragg peaks τ and superlattice peaks at $Q = \tau + q_i$ with $q_1 = (\frac{1}{4}, 0, 0)$, $q_2 = (0, \frac{1}{4}, 0)$ and $q_3 = (\frac{1}{4}, -\frac{1}{4}, 0)$. As the temperature decreases below $T_{CO,2}$, approximately 80 K, an additional set of reflections emerges at positions corresponding to $q'_1 = (\frac{1}{6}, 0, 0)$, $q'_2 = (0, \frac{1}{6}, 0)$, and $q'_3 = (\frac{1}{6}, -\frac{1}{6}, 0)$. Significantly, both $\frac{1}{4}$ and $\frac{1}{6}$ charge orders coexist below 80 K, persisting into the superconducting state. Figure 1a illustrates a schematic diagram showing the evolution of structural and electronic properties with respect to temperature. The diagram captures the progression of the material through a structural phase transition from the high-temperature hexagonal $P6/mmm$ phase (SG No. 191) to the low-temperature orthorhombic $Cccm$

phase (SG No. 66) at $T_{str} \simeq 600$ K. Subsequently, it highlights the onset of primary ($\frac{1}{4}$) charge order at $T_{co,1} \simeq 400$ K and the emergence of secondary ($\frac{1}{6}$) charge order below $T_{co,2} \simeq 80$ K. Notably, both charge orders coexist with superconductivity, manifesting below 7 K.

The superconducting transitions in LaRu₃Si₂ were examined in electrical resistivity experiments with the magnetic field applied both perpendicular (Fig. 2a) and parallel (Fig. 2b) to the c axis. The results indicate a weak anisotropy of the second critical field H_{c2} . The estimated anisotropy of H_{c2} is approximately 1.25, a value significantly lower than the observed anisotropy of 8 in CsV₃Sb₅. In our investigation of the electronic properties of LaRu₃Si₂ in its normal state, comprehensive macroscopic magnetization and resistivity measurements were conducted under the influence of an applied magnetic field. Figure 3a illustrates the temperature dependence of magnetic susceptibility at a magnetic field strength of 1 T, both parallel and perpendicular to the c axis. When the magnetic field is applied parallel to the c axis ($H \parallel c$), three distinct anomalies in the magnetic susceptibility are observed. Initially, a subtle drop in susceptibility occurs around 350 K, closely associated with the onset of the primary charge order at $T_{co,1}$. Subsequently, a sharp increase is evident below the secondary charge-order temperature $T_{CO,2}$, approximately 80 K, followed by an additional notable increase below $T^* \approx 35$ K. Interestingly, these magnetic susceptibility anomalies are prominently observed when the magnetic field is aligned along the c axis, but they are significantly less discernible when the field is applied in the kagome plane. In the case of $H \perp c$, only the transition at T^* is evident. This indicates that the magnetic response across the charge-order temperatures is anisotropic. The corresponding temperatures are highlighted in Figure 3b, where the temperature-dependent resistivity under zero field, as well as its derivative, are presented. The derivative of the resistivity exhibits a peak at T^* , while a subtle change in the slope of the resistivity curve is observed across the charge ordering temperatures $T_{co,1}$ and $T_{CO,2}$.

The magnetotransport data obtained for LaRu₃Si₂ of

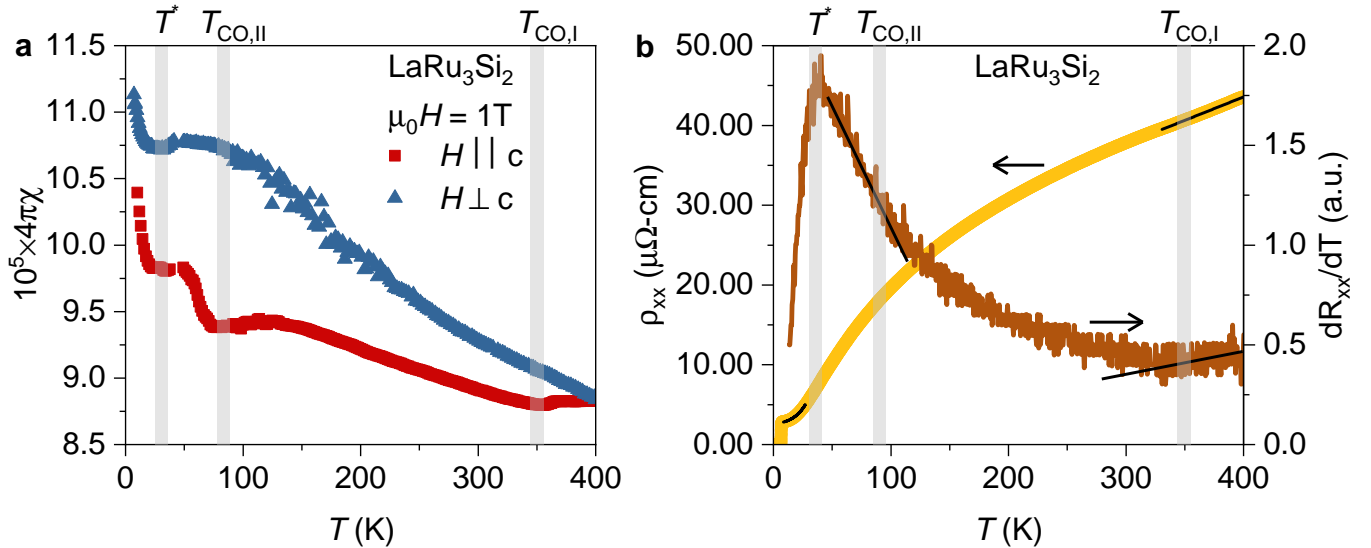


Figure 3: **Magnetic and transport anomalies in LaRu_3Si_2 .** **a**, The temperature dependence of magnetic susceptibility, measured under the magnetic field of 1 T, applied parallel and perpendicular to c -axis. **b**, Temperature dependence of the normal state longitudinal resistance ρ_{xx} and its first derivative. Vertical grey lines mark three characteristic temperatures T^* , $T_{\text{co,I}}$ and $T_{\text{co,II}}$.

fer compelling evidence of the low-temperature charge-order transition. Magnetotransport [43–45], known for its sensitivity in detecting charge-order transitions, utilizes magnetoresistance (MR) as a measure of the mean free path integrated over the Fermi surface [46]. This method is particularly adept at detecting changes in scattering anisotropy and Fermi surface reconstructions. In Figure 4a, we present the MR under a perpendicular magnetic field in LaRu_3Si_2 across the temperature range of 10 K to 70 K. Within the primary $\frac{1}{4}$ charge-ordered state, MR remains zero, only emerging below the $\frac{1}{6}$ charge ordering temperature $T_{\text{CO},2}$. The MR exhibits an initial increase at $T_{\text{CO},2}$, with a faster increase below T^* , see Fig. 4b. We note that not only does the absolute value of MR alter with decreasing temperature, but the overall profile of MR also undergoes modification as the temperature decreases.

The Kohler plot, $\Delta\rho/\rho_{H=0}$ vs $(\mu_0 H/\rho H = 0)^2$, displayed in Figure 4c, is particularly noteworthy. The interesting observation in the Kohler plot is the singular behavior, where the MR data converge to a single line only below 15 K, in stark contrast to the pronounced temperature dependence evident at higher temperatures. Kohler’s rule is a general principle stating that the normalized magnetoresistance, when plotted against a normalized magnetic field, should yield a universal curve for metals with simple Fermi surfaces. This principle tends to hold true even in materials with complex Fermi surfaces, provided there are no temperature-dependent changes in the details of the Fermi surface. The deviation from the Kohler’s rule in LaRu_3Si_2 suggests a fundamental alteration in the electronic structure and scattering processes associated with the onset of secondary charge order, emphasizing its significant impact on the

transport properties of the material.

To further elucidate the electronic properties, Hall measurements were conducted, revealing a linear Hall resistivity at all temperatures. A linear Hall effect implies that transport is predominantly governed by a single type of charge carrier. In Figure 4d, the Hall effect exhibits a pronounced temperature-dependence below $T_{\text{CO},2}$, with the sign of the Hall signal transitioning smoothly from positive (holes) to negative (electrons) across T^* . These findings contribute valuable insights into the charge-order-induced alterations in the electronic structure of LaRu_3Si_2 . The sign reversal observed across the charge-ordering temperature in LaRu_3Si_2 parallels findings previously reported in 2H-NbSe_2 [47] and cuprate high-temperature superconductors [48, 49]. In those cases, this behavior was interpreted as a consequence of Fermi-surface reconstruction associated with the onset of a density-wave phase. It appears that in LaRu_3Si_2 , the emergence of the secondary charge order similarly triggers a reconstruction of the Fermi surface, resulting in the appearance of an electron pocket. The similarities in the observed phenomena across different materials suggest a common underlying mechanism linked to charge order-induced alterations in the electronic structure.

Subsequently, motivated by the significant magnetoresistance at low temperatures in LaRu_3Si_2 and the magnetic response reported in the charge-ordered state of other kagome-lattice superconductors [13, 14, 23, 26, 27], we conducted zero-field and high-field μSR (muon spin rotation) experiments on a single crystalline sample of LaRu_3Si_2 . The zero-field (ZF)- μSR spectrum (Fig. 5a) is characterized by a weak depolarization of the muon spin ensemble, indicating no evidence of long-range or-

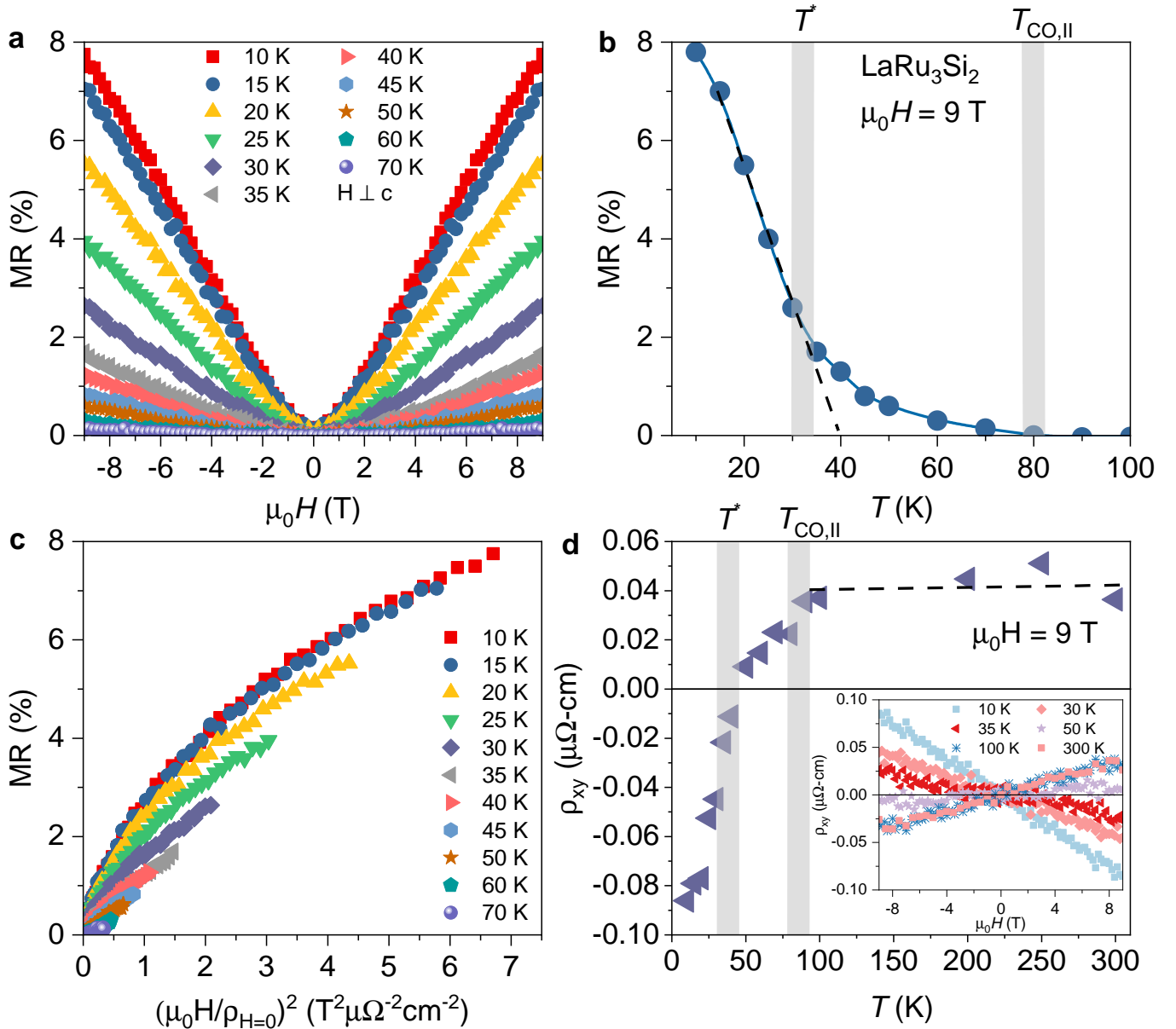


Figure 4: **Magnetotransport characteristics for LaRu_3Si_2 .** **a**, The magnetoresistance measured at various temperatures across the charge ordering temperature $T_{\text{CO},2} \simeq 80$ K. **b**, The temperature dependence of the value of magnetoresistance at 9 T. **c**, Kohler plot, $\Delta\rho/\rho_{H=0}$ vs $(\mu_0 H/\rho_{H=0})^2$, of the magnetoresistance, plotted from field-sweeps at various temperatures. **d**, The temperature dependence of the value of the Hall resistance ρ_{xy} at 9 T. Inset shows the Hall resistance, measured at various temperatures between 10 K and 300 K.

dered magnetism in LaRu_3Si_2 . However, it shows that the muon spin relaxation has a clearly observable temperature dependence. Since the full polarization can be recovered by the application of a small external longitudinal magnetic field, $B_{\text{LF}} = 5$ mT, the relaxation is, therefore, due to spontaneous fields which are static on the microsecond timescale. The zero-field μSR spectra for LaRu_3Si_2 were fitted using the simple exponential function $P_{\text{ZF}}(t) = \exp(-\Gamma_{\text{ZF}}t)$. Across the charge ordering temperature $T_{\text{CO},2} \simeq 80$ K, there is only a change in the slope of Γ . However, a more significant observa-

tion occurs as the temperature is lowered below $T^* \simeq 35$ K, where there is a notable increase in Γ . A possible reason for the change of the relaxation rate across T^* could be an additional modulation of the lattice structure that slightly alters the nuclear positions around the muon [50]. However, a rough order of magnitude estimate yields that the structural distortions of the order of 0.1 Å for the atoms closest to the muon would be needed to explain the observed effect in the second moment of the measured field distribution. This is a large effect that has not been seen by X-ray diffraction experiments.

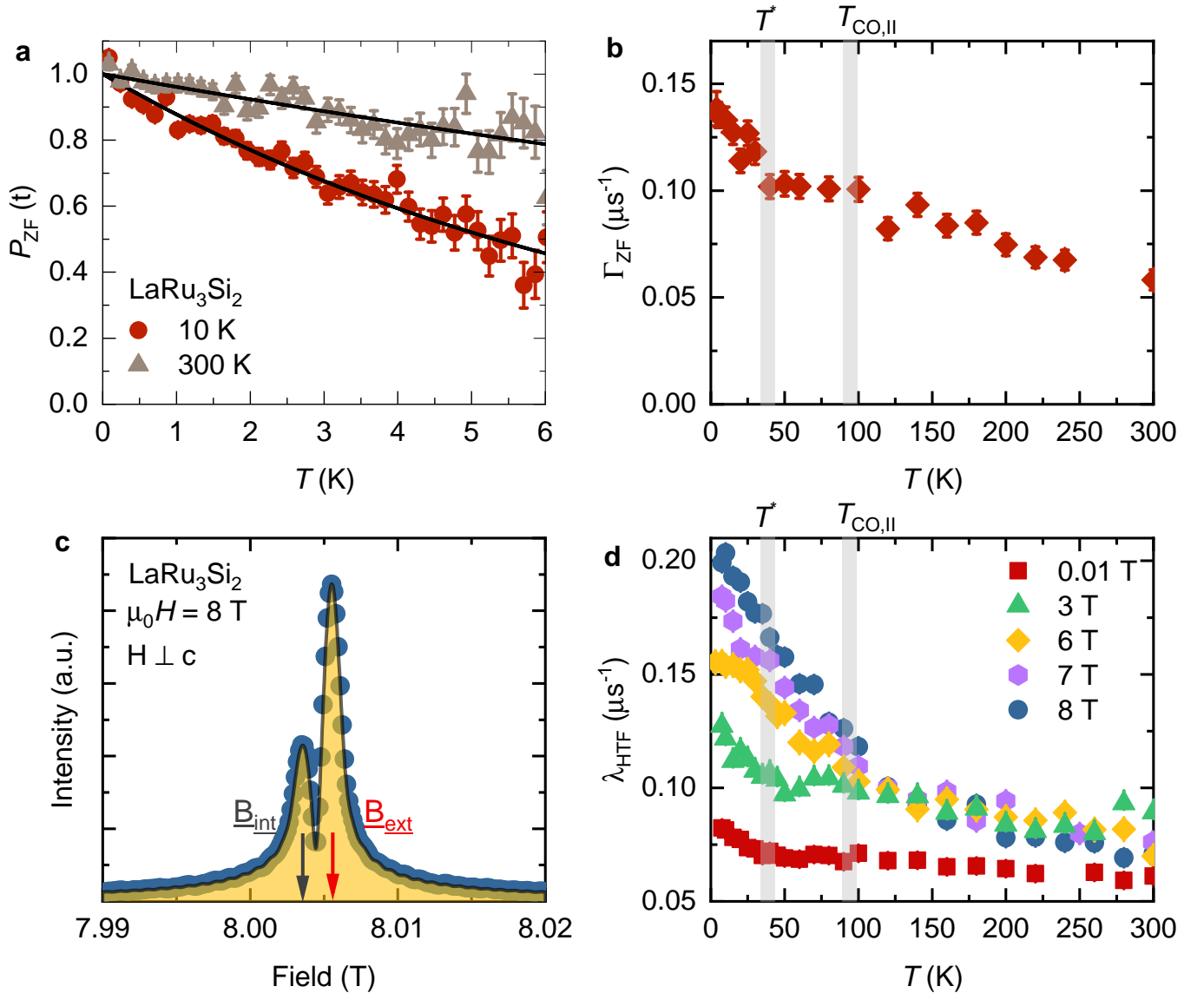


Figure 5: **Magnetic response of the charge order in zero-field and applying external magnetic fields in LaRu_3Si_2 .** **a**, The ZF μSR time spectra, obtained at $T = 10\text{ K}$ and 300 K , all above the superconducting transition temperature T_c . The solid black curves in panel **a** represent fits to the recorded time spectra, using the simple exponential function. Error bars are the standard error of the mean (s.e.m.) in about 10^6 events. **b**, The temperature dependences of the zero-field muon spin relaxation rate Γ_{ZF} , obtained over a wide temperature range. The error bars represent the standard deviation of the fit parameters. **c**, Fourier transform of the μSR asymmetry spectra for the single crystal of LaRu_3Si_2 at 5 K in the presence of an applied field of $\mu_0 H = 8\text{ T}$. The solid line is a two-component signal fit. The peaks marked by the arrows denote the external and internal fields, determined as the mean values of the field distribution from the silver sample holder and from the sample, respectively. The short-time-window apodization function was used in the Fourier transform amplitude plot. **d**, Temperature dependence of the high transverse field muon spin relaxation rate λ_{HTF} for the single crystal of LaRu_3Si_2 , measured under different c -axis magnetic fields. The vertical grey line marks the transition temperature below which the field effect was observed. The error bars represent the standard deviation of the fit parameters.

Therefore, we can dismiss the structural distortion being the origin for the increase of the relaxation rate. Most importantly, our high-field μSR results presented here definitively prove that there is indeed a strong contribution of electronic origin to the muon spin relaxation below the charge-ordering temperature (see below). Therefore, we interpret our ZF- μSR results as an indication that

there is an enhanced width of internal fields sensed by the muon ensemble below $T^* \simeq 35\text{ K}$. The increase in Γ below T^* is estimated to be $\simeq 0.035\ \mu\text{s}^{-1}$, which can be interpreted as a characteristic field strength $\Gamma/\gamma_\mu \simeq 0.4\text{ G}$.

To corroborate the zero-field μSR results presented above, a comprehensive set of high-field μSR experiments

was conducted [51]. Figure 5c illustrates the probability field distribution measured at 5 K in a magnetic field of 8 T applied perpendicular to the crystallographic c axis. Throughout the investigated temperature range, the μ SR signals were characterized by two components: a signal with fast relaxation ($\lambda_{\text{HTF}} \simeq 0.428(3) \mu\text{s}^{-1}$) and another with slower relaxation ($0.05 \mu\text{s}^{-1}$). The fast relaxation signal, predominant in the μ SR spectrum, arises from muons stopping within the sample and indicates a bulk response. Fig. 5d depicts the behavior of the relaxation rate in a magnetic field of 0.01 T applied parallel to the c axis, resembling the temperature dependence observed in zero-field conditions. At higher fields (3 T, 6 T, 7 T, and 8 T), the temperature dependence of the relaxation rate varies, with a clear and monotonous increase below the onset temperature $T_{\text{CO},2}$. This suggests that the low-temperature relaxation rate in magnetic fields is predominantly influenced by electronic/magnetic contributions, as nuclear contributions are not susceptible to external field enhancement. The absolute increase of the relaxation rate between the onset of charge order $T_{\text{CO},2}$ and the base temperature in 8 T is $\Delta\lambda_{\text{HTF}} \simeq 0.1 \mu\text{s}^{-1}$, which is smaller than in other kagome-lattice superconductors such as KV_3Sb_5 [13] and ScV_6Sn_6 [20]. Since the onset of the weak magnetic response aligns with the temperature $T_{\text{CO},2}$ of $(\frac{1}{6}, 0, 0)$ charge order, this indicates a strong intertwining between magnetic and charge channels. Additionally, a weak but non-negligible field effect on the relaxation rate is observed above $T_{\text{CO},2}$, extending up to at least 300 K. This effect may be associated with the high-temperature charge-ordered state, and further experiments above 300 K are crucial for a more comprehensive understanding.

In this paper, we have presented three main findings: (1) Charge order with a propagation vector of $(\frac{1}{6}, 0, 0)$ is identified in the single crystal of LaRu_3Si_2 below a critical temperature $T_{\text{CO},2} \simeq 80$ K, coexisting with a previously reported room-temperature primary charge order $(\frac{1}{4}, 0, 0)$. The charge order persists into the superconducting state, highlighting the intricate interplay between superconductivity and distinct charge-order phenomena. (2) Magnetotransport measurements reveal zero magnetoresistance within the primary charge-ordered state and the appearance of magnetoresistance below $T_{\text{CO},2}$. The Kohler plot analysis, showing a violation of Kohler's rule, suggests a Fermi surface reconstruction induced by charge order. Anomalies in the Hall resistivity and its sign reversal across the charge-ordering temperature further indicate a complex interplay of electronic states. The reconstruction of the Fermi surface is a fundamental aspect of such phenomena, wherein the charge order induces changes in the distribution of electronic states near the Fermi level. This restructuring can lead to anomalous transport properties, such as the observed temperature-dependent Hall resistance and its sign reversal. By drawing parallels to observations in other materials such as cuprate high temperature superconductors, the study of LaRu_3Si_2 provides valuable insights into the universal

aspects of charge order effects on electronic behavior, contributing to the broader understanding of quantum materials. (3) The μ SR experiments conducted in both zero-field and high-field conditions have yielded noteworthy insights into the properties of LaRu_3Si_2 . Below T^* , approximately 35 K, there is a notable enhancement in the internal field width sensed by the muon ensemble. Additionally, a pronounced field-induced enhancement of the relaxation rate is observed below $T_{\text{CO},2}$, which is around 80 K. These observations collectively indicate time-reversal symmetry breaking within the secondary charge-ordered state.

The debate about the origins [52] of the various forms of charge order found in Kagome systems focuses on whether they are caused by electronic interactions or phononic effects. Electronically, there is significant interest in how sublattice interference and Q vectors connect the van Hove singularities (vHS) [4, 32]. The proximity of VHS to the Fermi level is key to the unusual superconductivity and 2×2 charge order in the AV_3Sb_5 ($A=\text{K, Rb, Cs}$) compounds [12]. This 2×2 charge order pattern is also observed in the magnetic Kagome lattice of FeGe [21, 22], exhibiting similarities with the charge order found in Kagome superconductors AV_3Sb_5 . In ScV_6Sn_6 [19], the band structure also shows vHS near the Fermi level, but its charge order differs from the AV_3Sb_5 series. In ScV_6Sn_6 [19], the primary driver for charge order is believed to be phonons, with the leading distortion involving an out-of-plane modulation of Sn and Sc sites [53–56]. This is in contrast to the in-plane Kagome breathing mode in AV_3Sb_5 . The Kagome superconductor LaRu_3Si_2 also has vHS in its band structure, relating to $\text{Ru-}d_{z^2}$ orbitals near the Fermi level [8]. Its charge order [5] involves the in-plane displacement of Si atoms and out-of-plane displacements of some Ru atoms, differentiating it from both AV_3Sb_5 and ScV_6Sn_6 . Additionally, the superconductor LaRu_3Si_2 exhibits a distinctive three-dimensional character, both in its band structure and in its isotropic superconducting properties. This contrasts with the more two-dimensional nature of the AV_3Sb_5 . Despite these variations in charge-order structures and their formation mechanisms (electronic and phononic) in different Kagome superconductors, they commonly exhibit indications of time-reversal symmetry breaking in the charge-ordered state [13, 14, 20, 23, 26]. This suggests a prevalent occurrence of time-reversal symmetry-breaking in charge-ordered Kagome lattices, transcending specific fermiologies. LaRu_3Si_2 is unique among Kagome superconductors for its coexistence of multiple charge orders, each with distinct magnetic responses. It might be conjectured that the high-temperature transitions at T_{str} and $T_{\text{CO},1}$ are phonon-driven, while for the low-temperature transition at $T_{\text{CO},2}$, electronic interactions are relevant. These findings deepen our understanding of how lattice and electronic effects interact to cause charge order instabilities in these complex systems. The presence of various orders at different temperatures might relate to orbitally selective ordering, adding complexity

to the understanding of these materials' electronic and magnetic properties and highlighting distinctiveness of LaRu₃Si₂ in the Kagome superconductor family.

I. METHODS

X-ray diffraction: X-ray diffraction was performed at ID27, ESRF using monochromatic x-rays with a wavelength of 0.3738 Å and a spotsize of 0.6x0.6 μm². The sample was mounted on a membrane driven diamond anvil cell with 70 degrees angular aperture designed at ESRF. Helium was used as pressure transmitting medium and the applied pressure was measured by Ruby fluorescence. The diamond anvil cell was mounted into a Helium flow cryostat (ESRF). The applied pressure was kept constant to 0.3 GPa during cooling by adapting the membrane pressure. X-ray diffraction was collected with a Eiger2 CdTe detector (DECTRIS AG, Baden-Daettwil, Switzerland) in shutterless mode and continuous rotation over 64 degrees with readout every 0.1 degree. CrysAlisPro (Rigaku) was used for data reduction and reciprocal space reconstructions. Our prior measurements using muon spin rotation revealed that applying pressures up to 2.2 GPa does not change the physical properties of this material. This suggests that a pressure of 0.3 GPa can be regarded as the ambient pressure for LaRu₃Si₂.

Magnetotransport: The magnetoresistance of the single-crystal LaRu₃Si₂ was assessed using the physical property measurement system (PPMS-9, Quantum Design) employing the conventional four-probe technique. Four Pt-wires (0.0254 mm diameter) were affixed to the single crystal using silver epoxy, forming a bar-shaped specimen after polishing. A constant electrical current of 1 mA was applied, and the magnetic field was directed along the crystallographic *a*- and *c*-axes, a configuration validated through Laue measurement.

μSR experiment: In a μSR (muon spin rotation) experiment, nearly 100% spin-polarized muons μ⁺ are introduced into the sample one at a time. These positively charged μ⁺ particles thermally stabilize at interstitial lattice sites, effectively serving as magnetic microprobes within the material. In the presence of a magnetic field, the muon spin undergoes precession at the local field B_μ at the muon site, with a Larmor frequency ν_μ given by $\gamma_\mu/(2\pi)B_\mu$, where $\gamma_\mu/(2\pi)$ represents the muon gyromagnetic ratio and is equal to 135.5 MHz T⁻¹.

Zero field (ZF) and transverse field (TF) μSR experiments on the single crystalline sample of LaRu₃Si₂ were performed on the GPS instrument and high-field HAL-

9500 instrument, equipped with BlueFors vacuum-loaded cryogen-free dilution refrigerator (DR), at the Swiss Muon Source (SμS) at the Paul Scherrer Institut, in Villigen, Switzerland. Large single crystal piece was used for these measurements. The crystal, with dimensions 7×1.7×0.7 mm³, was affixed to a 5 mm circular silver sample holder using a small droplet of GE varnish during high-field experiments. The magnetic field was applied perpendicular to the crystallographic *c*-axis. The crystal was mounted such that the *c*-axis of it is perpendicular to the muon beam. Using the "spin rotator" at the πM3 beamline, muon spin was rotated (from its natural orientation, which is antiparallel to the momentum of the muon) by 44.5(3)° degrees with respect to the *c*-axis of the crystal. So, the sample orientation is fixed but the muon spin was rotated. The rotation angle can be precisely determined to be 44.5(3)° by measurements in weak magnetic field, applied transverse to the muon spin polarization. Zero field and high transverse field μSR data analysis on single crystals of LaRu₃Si₂ were performed using both the so-called asymmetry and single-histogram modes [57, 58]. The experimental data were analyzed using the MUSRFIT package [57].

II. ACKNOWLEDGMENTS

The μSR experiments were carried out at the Swiss Muon Source (SμS) Paul Scherrer Institute, Villigen, Switzerland. X-ray diffraction experiments were performed at ID27 at European Synchrotron Radiation Facility (ESRF), France. Z.G. acknowledges support from the Swiss National Science Foundation (SNSF) through SNSF Starting Grant (No. TMSGI2_211750). Z.G. acknowledges the useful discussions with Robert Scheuermann. I.P. acknowledges support from Paul Scherrer Institute research grant No. 2021_0134.

Author Contributions Z.G. conceived and supervised the project. Growth of the single crystal LaRu₃Si₂: H.N., and S.N.. Single crystal X-ray diffraction experiments, analysis and corresponding discussions: B.W., C.M.III, I.P., V.S., S.S., J.N.G., G.G., J.K., I.B., J.C., E.P., D.J.G., and Z.G.. Magnetotransport experiments: V.S., M.B., and Z.G.. Magnetization experiments: C.M.III, M.M., D.J.G., and Z.G. Muon spin rotation experiments and the corresponding discussions: C.M.III, V.S., J.N.G., D.D., S.S.I., M.H.F., T.N., J.-X.Y., M.Z.H., H.L., R.K., and Z.G.. Figure development: V.S., C.M.III, and Z.G.. Writing of the paper: Z.G. with contributions from all authors. All authors discussed the results, interpretation and conclusion.

[1] Syōzi, I. Statistics of Kagome Lattice. *Prog. Theor. Phys.* **6**, 306 (1951).

[2] Yin, J.-X., Lian, B. and Hasan, M.Z.. Topological

- kagome magnets and superconductors. *Nature* **612**, 647-657 (2022).
- [3] Guguchia, Z. et al. Tunable anomalous Hall conductivity through volume-wise magnetic competition in a topological kagome magnet. *Nature Communications* **11**, 559 (2020).
 - [4] Kiesel, M.L. and Thomale, R. Sublattice interference in the kagome Hubbard model. *Phys. Rev. B* **86**, 121105 (2012).
 - [5] Plokhikh, I. et al. and Guguchia, Z. Charge order above room-temperature in a prototypical kagome superconductor $\text{La}(\text{Ru}_{1-x}\text{Fe}_x)_3\text{Si}_2$. arXiv:2309.09255 (2023).
 - [6] Barz, H. Ternary transition metal phosphides: High-temperature superconductors. *Mater. Res. Bull. PNAS* **15**, 1489 (1980).
 - [7] Vandenberg, J.M. and Barz, H. *ibid.* **15**, 1493 (1980).
 - [8] Mielke III, C. et al. Nodeless kagome superconductivity in LaRu_3Si_2 . *Phys. Rev. Mat.* **5**, 034803 (2021).
 - [9] Ortiz, B. et al. CsV_3Sb_5 : A Z_2 Topological Kagome Metal with a Superconducting Ground State. *Phys. Rev. Lett.* **125**, 247002 (2020).
 - [10] Ortiz, B., Sarte, P., Kenney, E., Graf, M., Teicher, S., Seshadri, R., & Wilson, S. Superconductivity in the Z_2 kagome metal KV_3Sb_5 . *Phys. Rev. Materials* **5**, 034801 (2021).
 - [11] Yin, Q., Tu, Z., Gong, C., Fu, Y., Yan, S., & Lei, H. Superconductivity and normal-state properties of kagome metal RbV_3Sb_5 single crystals. *Chinese Phys. Lett.* **38**, 037403 (2021).
 - [12] Jiang, Y.-X. et al. Discovery of topological charge order in kagome superconductor KV_3Sb_5 . *Nature Materials* **20**, 1353-1357 (2021).
 - [13] Mielke III, C. et al., and Guguchia, Z. Time-reversal symmetry-breaking charge order in a kagome superconductor. *Nature* **602**, 245-250 (2022).
 - [14] Guguchia, Z., Khasanov, R. and Luetkens, H. Unconventional charge order and superconductivity in kagome-lattice systems as seen by muon-spin rotation. *npj Quantum Materials* **8**, 41 (2023).
 - [15] Neupert, T., Denner, M.M., Yin, J.-X., Thomale, R., and Hasan, M.Z.. Charge order and superconductivity in kagome materials. *Nature Physics* **18**, 137-143 (2022).
 - [16] Christensen, M.H., Birol, T., Andersen, B.M., Fernandes, R.M. Loop currents in AV_3Sb_5 kagome metals: multipolar and toroidal magnetic orders. *Phys. Rev. B* **106**, 144504 (2022).
 - [17] Wagner, G., Guo, C., Moll, Philip J.W., Neupert, T. and Fischer, M.H.. Phenomenology of bond and flux orders in kagome metals. *Phys. Rev. B* **108**, 125136 (2023).
 - [18] Grandi, F. et al. Theory of nematic charge orders in kagome metals. *Phys. Rev. B* **107**, 155131 (2023).
 - [19] Suriya Arachchige, H.W. et al. Charge density wave in kagome lattice intermetallic ScV_6Sn_6 . *Physical Review Letters* **129**, 216402 (2022).
 - [20] Guguchia, Z. et al., Hidden magnetism uncovered in charge ordered bilayer kagome material ScV_6Sn_6 . *Nature Communications* **14**, 7796 (2023).
 - [21] Yin, J.-X. et al., Discovery of Charge Order and Corresponding Edge State in Kagome Magnet FeGe . *Phys. Rev. Lett.* **129**, 166401 (2022).
 - [22] Teng, X et al., Magnetism and charge density wave order in kagome FeGe . *Nature Physics* **19**, 814-822 (2023).
 - [23] Guguchia, Z. et al., Tunable unconventional kagome superconductivity in charge ordered RbV_3Sb_5 and KV_3Sb_5 . *Nature Communications* **14**, 153 (2023).
 - [24] Shumiya, N. et al. Tunable chiral charge order in kagome superconductor RbV_3Sb_5 . *Phys. Rev. B* **104**, 035131 (2021).
 - [25] Wang, Z. et al. Electronic nature of chiral charge order in the kagome superconductor CsV_3Sb_5 . *Phys. Rev. B* **104**, 075148 (2021).
 - [26] Khasanov, R. et al. Time-reversal symmetry broken by charge order in CsV_3Sb_5 . *Phys. Rev. Research* **4**, 023244 (2022).
 - [27] Yu, L. et al. Evidence of a hidden flux phase in the topological kagome metal CsV_3Sb_5 . arXiv:2107.10714 (2021).
 - [28] Xu, Y. et al. Three-state nematicity and magneto-optical Kerr effect in the charge density waves in kagome superconductors. *Nature Physics* **18**, 1470-1475 (2022).
 - [29] Guo, C et al. Switchable chiral transport in charge-ordered kagome metal CsV_3Sb_5 . *Nature* **611**, 461-466 (2022).
 - [30] Yang, S. et. al., Giant, unconventional anomalous Hall effect in the metallic frustrated magnet candidate, KV_3Sb_5 . *Sci. Adv.* **6**, 1-7s (2020).
 - [31] Yu, F. et. al., Concurrence of anomalous Hall effect and charge density wave in a superconducting topological kagome metal. *Phys. Rev. B* **104**, 041103 (2021).
 - [32] Denner, M., Thomale, R., Neupert, T. Analysis of charge order in the kagome metal AV_3Sb_5 ($A = \text{K}, \text{Rb}, \text{Cs}$). *Phys. Rev. Lett.* **127**, 217601 (2022).
 - [33] Christensen, M.H., Birol, T., Andersen, B.M., Fernandes, R.M. Theory of the charge-density wave in AV_3Sb_5 kagome metals. *Phys. Rev. B* **104**, 214513 (2021).
 - [34] Ritz, E.T., Fernandes, R.M., Birol, T. Impact of Sb degrees of freedom on the charge density wave phase diagram of the kagome metal CsV_3Sb_5 . Preprint at <https://arxiv.org/abs/2212.13319> (2022).
 - [35] Tazai, R., Yamakawa, Y., Onari, S., Kontani, H. Mechanism of exotic density-wave and beyond-Migdal unconventional superconductivity in kagome metal AV_3Sb_5 ($A=\text{K}, \text{Rb}, \text{Cs}$). *Sci. Adv.* **8**, eabl4108 (2022).
 - [36] Park, T., Ye, M., Balents, L. Electronic instabilities of kagome metals: Saddle points and Landau theory. *Phys. Rev. B* **104**, 035142 (2021).
 - [37] Lin, Y.-P. and Nandkishore, R.M. Complex charge density waves at Van Hove singularity on hexagonal lattices: Haldane-model phase diagram and potential realization in the kagome metals AV_3Sb_5 . *Phys. Rev. B* **104**, 045122 (2021).
 - [38] Chandan Setty, C., Hu, H., Chen, L., Si, Q. Electron correlations and T -breaking density wave order in a Z_2 kagome metal, <https://arxiv.org/abs/2105.15204> (2021).
 - [39] Kishimoto, Y., Ohno, T., Hihara, T., Sumiyama, K., Ghosh, G., and Gupta, L.C. Magnetic Susceptibility Study of LaRu_3Si_2 . *J. Phys. Soc. Jpn.* **71**, 2035-2038 (2002).
 - [40] Li, B., Li, S. and Wen, H.-H. Chemical doping effect in the LaRu_3Si_2 superconductor with a kagome lattice. *Phys. Rev. B* **94**, 094523 (2016).
 - [41] Li, S. et. al., Anomalous Properties in the Normal and Superconducting States of LaRu_3Si_2 . *Phys. Rev. B* **84**, 214527 (2011).
 - [42] Electronic Correlation Effects on Stabilizing a Perfect Kagome Lattice and Ferromagnetic Fluctuation in LaRu_3Si_2 . *JUSTC* **53**, 0702 (2023).
 - [43] Giraldo-Gallo, P. et al. Scale-invariant magnetoresistance in a cuprate superconductor. *Science* **361**, 479-481

- (2018).
- [44] Novak, M., Sasaki, S., Segawa, K., and Ando, Y. Large linear magnetoresistance in the Dirac semimetal TlBiSSe. *Phys. Rev. B* **91**, 041203(R) (2015).
- [45] Wei, X. et al. Linear nonsaturating magnetoresistance in kagome superconductor CsV₃Sb₅ thin flakes. Preprint at <https://arXiv:2210.16890> (2022).
- [46] Das, L. et al. Two-carrier Magnetoresistance: Applications to Ca₃Ru₂O₇. *J. Phys. Soc. Jpn.* **90**, 054702 (2021).
- [47] Li, L., Shen, J., Xu, Z., and Wang, H. Magnetoresistance and Hall Effect of Two-Dimensional 2H-NbSe₂. *International Journal of Modern Physics B* **19**, 275-279 (2005).
- [48] LeBoeuf, D. et al., Electron pockets in the Fermi surface of hole-doped high- T_c superconductors. *Nature* **450**, 533-536 (2007).
- [49] LeBoeuf, D. et al., Lifshitz critical point in the cuprate superconductor YBa₂Cu₃O_y from high-field Hall effect measurements. *Phys. Rev. B* **83**, 054506 (2011).
- [50] Bonfa, P. Entanglement between Muon and $I > 1/2$ Nuclear Spins as a Probe of Charge Environment. *Phys. Rev. Lett.* **129**, 097205 (2022).
- [51] Sedlak, K., Scheuermann, R., Stoykov, A., Amato, A. GEANT4 simulation and optimisation of the high-field μ SR spectrometer. *Physica B* **404**, 970-973 (2009).
- [52] Johannes, M.D. and Mazin, I.I. Fermi surface nesting and the origin of charge density waves in metals. *Phys. Rev. B* **77**, 165135 (2008).
- [53] Cao, S et al. Competing charge-density wave instabilities in the kagome metal ScV₆Sn₆. Preprint at <https://arXiv:2304.08197v1>.
- [54] Hu, H. et al. Kagome Materials I: SG 191, ScV₆Sn₆. Flat Phonon Soft Modes and Unconventional CDW Formation: Microscopic and Effective Theory. Preprint at <https://arXiv:2305.15469> (2023).
- [55] Yong, H. et al. Phonon promoted charge density wave in topological kagome metal ScV₆Sn₆. Preprint at [https://arXiv:\(2023\)](https://arXiv:(2023)).
- [56] Korshunov, A et al. Softening of a flat phonon mode in the kagome ScV₆Sn₆. *Nat. Commun.* **14**, 6646 (2023).
- [57] Suter, A. and Wojek, B.M. Musrfit: A Free Platform-Independent Framework for μ SR Data Analysis. *Physics Procedia* **30**, 69 (2012).
- [58] Yaouanc, A. & Dalmas de Reotier, P. Muon Spin Rotation, Relaxation, and Resonance: Applications to Condensed Matter. Oxford University Press (2011).